CRYSTAL STRUCTURES OF BIOTITE AT HIGH TEMPERATURES AND OF HEAT-TREATED BIOTITE USING NEUTRON POWDER DIFFRACTION

Chul-Min Chon[1], Shin Ae Kim[2] and Hi-Soo Moon[1,*]

[1] Department of Earth System Sciences, Yonsei University, Seoul 120-749, Korea
[2] Korea Atomic Energy Research Institute, Daejeon 305-600, Korea

Abstract—The crystal structure of biotite-1M from Bancroft, Ontario, with the formula: $(K_{1.96}Na_{0.13}Ca_{0.01})(Mg_{3.15}Fe^{2+}_{2.59}Ti_{0.17}Mn_{0.09})(Si_{5.98}Al_{1.92}Ti_{0.10})O_{20}[(OH)_{1.47}F_{1.98}]$, was determined by Rietveld refinement using high-resolution neutron powder diffraction at *in situ* temperatures ranging from 20 to 900ºC. The room-temperature structure of the samples heated to between 400 and 900ºC using an electric furnace in air was also refined. The crystal structures were refined to an R_P of 2.98 –5.06% and R_{wp} of 3.84 –6.77%. For the *in situ* heating experiments in a vacuum, the unit-cell dimensions increased linearly to 600ºC. The linear expansion coefficient for the c axis was 1.65×10^{-5}ºC^{-1}, while those for the a and b dimensions were 4.44×10^{-6}ºC^{-1} and 5.21×10^{-6}ºC^{-1}, respectively. Accordingly, the increase in the unit-cell volume up to 600ºC occurred mainly along the c axis, resulting from the expansion in the K coordination sphere along that direction. Results for all K –O bonds were analyzed in terms of the lattice component and an inner component of the structural strain. The ditrigonal distortion decreased (3.76º at 20ºC to 1.95º at 600ºC) with temperature, because the shorter bonds expanded and the longer bonds contracted. The increase in the interlayer separation and the decrease in the interlayer octahedral flattening angle confirmed that the c-dominated expansion occurred in the interlayer region. In the case of the *ex situ*-heated samples, the cell dimensions decreased sharply at temperatures over 400ºC. The octahedral sheet thickness and mean $<M–O>$ distance decreased linearly due to oxidation of octahedral Fe. However, the interlayer separation and mean $<K–O>$ distance decreased at temperatures over 400ºC. At 400ºC, dehydroxylation began to increase and interlayer regions became more constricted. The overall cell parameters decreased rapidly with increasing temperatures due to dehydroxylation. The large inner strain components in the K –O bonds also resulted in an increase in the considerable ditrigonal distortion (3.57º at 400ºC to 6.15º at 900ºC).

Key Words—Biotite, Crystal Structure, Iron Oxidation, Lattice and Inner Strain, Neutron Powder Diffraction.

INTRODUCTION

Biotite occurs in a great variety of geological environments. It is a trioctahedral mica with a large concentration of Fe^{2+} substituting for octahedral Mg^{2+}. The effect of temperature on the phlogopite–annite join associated with metamorphic or plutonic processes has attracted much interest. The crystal chemistry of biotite has been used to investigate the nature and significance of the metamorphic process (Bohlen *et al.*, 1980) and characterize plutonic complexes by crystal-structure refinements (Brigatti and Davoli, 1990; Bigi and Brigatti, 1994). Using Mössbauer spectroscopy, Virgo and Popp (2000) evaluated experimentally the substitutional mechanisms that control the Fe oxidation state in mantle-derived phlogopite.

To examine the temperature effect on the crystal structure of the phlogopite–annite join (biotite), temperature experiments were historically performed in air or in vacuum and the structure was studied by single-crystal X-ray diffraction (XRD). Takeda and Morosin

(1975) were the first to perform a high-temperature structural study of phlogopite. The study included a single-crystal structural analysis for a synthetic fluor-ophlogopite, and successfully related a geometrical model structure to the structural changes in mica at 700ºC. However, the model cannot be applied to predicting the structural changes in hydroxyl-rich micas. Russell and Guggenheim (1999) reported the structures of a hydroxyl-rich phlogopite up to 600ºC and a heat-treated, Fe-rich phlogopite (biotite) at 904ºC. They showed the influence of the (O, OH, F) sites at high temperatures in a single-crystal structural study. However, the work did not include a structural study of a biotite with an intermediate Fe/Mg ratio at the reported temperatures. Recently, while studying the Fe oxidation mechanisms of biotite, Rancourt *et al.* (2001) attempted to resolve the hydrogen loss and vacancy reactions in annite using many kinds of analytical techniques, but few results of a detailed crystal structure were reported. Determining the temperature effect of the biotite structure is difficult because of complications arising from the multiple oxidation states of the Fe and from dehydroxylation-oxidation reactions. The tetrahedral, octahedral and interlayer structural parameters on heat-treated biotite samples at different temperatures can

* E-mail address of corresponding author:
hsmoon@yonsei.ac.kr

519

provide useful information to understand better the temperature effect on the structure.

Many studies of the phyllosilicate structure using neutron powder diffraction, especially for the mica structure, have been reported. It has many advantages over XRD, such as weak absorption, high penetration and angle-independent scattering length. Much of the interest in using neutron diffraction has been because of its sensitivity to H (or D) and its ability to determine crystal structures accurately, including hydrogen positions. Some studies have examined the crystal structure of phlogopite and chlorite at room temperature, of kaolinite, and of deuterated kaolinite at low temperature (Joswig, 1972; Rayner, 1974; Joswig *et al.*, 1980; Bish, 1993; Akiba *et al.*, 1997). Either room temperature or low temperature is used when the accurate determination of crystal structures is required, such as in investigating the positions of H atoms in muscovite (Catti *et al.*, 1994; Liang and Hawthorne, 1998). Also, the octahedral occupancy in phengite (Pavese *et al.*, 2001) and the magnetism of synthetic and natural annite (Rancourt *et al.*, 1994), were studied using room/low-temperature neutron diffraction. Recent studies utilized high-temperature neutron powder diffraction when focusing on cation ordering and the stability of OH groups in phengite (Pavese *et al.*, 1997, 1999, 2000; Mookerjee *et al.*, 2001).

In the current study, the crystal structures of biotite were determined by Rietveld refinement from high-

resolution, high-temperature neutron powder diffraction. In addition, a structural study of *ex situ* furnace heating samples is reported. The changes in structural parameters as a function of temperature are examined in detail, and an attempt is made to determine the significance of the variations in the structure with relation to the Fe oxidation and dehydroxylation mechanism.

EXPERIMENTAL METHODS

Biotite from Bancroft, Ontario, was obtained from Wards Scientific Establishment, Inc. The sample was ground in a vibrating milling machine and passed through a 100 mesh sieve. The bulk chemical composition of the biotite sample was obtained to establish the structural formula using X-ray fluorescence (XRF, Philips, PW 2400) at the Korea Basic Science Institute. The OH^- concentration was determined by thermal gravimetric differential thermal analysis (TG/DTA, MAC Science, TG-DTA 2000S) on ~50 mg of powder heated at a rate of 10°C/min in N_2 gas to prevent Fe oxidation.

Neutron powder diffraction data were obtained using a high-resolution powder diffractometer in the HANARO reactor, Korea Atomic Energy Research Institute. The neutron wavelength was 1.8438Å, which was selected by a Ge(331) monochromator, and a vanadium can (Φ12mm, L55mm) was used as the sample

Table 1. Experimental details and final parameters of structure refinements.

	In situ experiments					Ex situ experiments				
Temperature (°C)	20	300	450	600	900	400	500	700	800	900
Neutron data collection and least squares parameters										
2θ scan range					20–155°					
Step size					0.05					
No. of steps					2700					
Max. intensity	34046	21981	13259	17887	15489	24572	34046	21981	17887	15489
No. of fitted parameters	47	46	47	46	46	47	47	47	47	47
No. of unique reflections	346	351	354	354	354	346	347	345	345	345
N – P + C	2652	2653	2652	2653	2653	2652	2652	2652	2652	2652
Refinement index (R index)										
R_p (%)	2.98	3.76	3.32	3.64	4.75	3.34	3.98	4.86	5.05	5.06
R_{wp} (%)	3.84	4.88	4.27	4.73	6.36	4.46	5.23	6.39	6.68	6.77
R_{exp} (%)	1.16	1.39	1.65	1.46	1.64	1.07	1.68	1.81	1.84	1.48
S (G. of F.)	3.31	3.51	2.59	3.24	3.89	4.17	3.11	3.53	3.63	4.57
R_B (%)	5.63	8.72	8.57	8.98	12.3	5.62	5.34	6.18	6.60	7.46
R_F (%)	4.24	5.74	5.89	6.02	7.63	3.87	3.57	4.07	4.54	5.12
DW statistics	0.2763	0.2362	0.6717	0.2654	0.1971	0.1970	0.2995	0.2458	0.2180	0.1568
FWHM (full width at half maximun)										
U	0.741	0.75	0.735	0.899	0.956	0.683	0.923	0.777	0.669	0.647
V	−0.858	−0.854	−0.784	−0.972	−1.104	−0.628	−0.771	−0.824	−0.744	−0.697
W	0.424	0.395	0.383	0.429	0.485	0.348	0.495	0.413	0.380	0.366

Note: N–P+C = no. of observation(steps) – no. of least-squares parameters + no. of phase, $R_p = 100 \times |Y_{io} - Y_{ic}|/Y_{io}$ (R-pattern), $R_{wp} = 100 \times [w_i(Y_{io} - Y_{ic})^2/w_i Y_{io}^2]^{1/2}$ (R weighted pattern), $R_{exp} = [(N - P)/w_i Y_{io}^2]^{1/2}$ (R expected pattern), $R_B = 100 \times ||I_{Ko}| - |I_{Kc}||/|I_{Ko}|$ (R Bragg factor), $R_F = 100 \times ||I_{Ko}|^{1/2} - |I_{Kc}|^{1/2}|/|I_{Ko}|^{1/2}$ (R structure factor), $H^2 = U\tan2\theta + V\tan\theta + W$ (according to Young, 1993)

holder. Profiles were taken from the 2θ range between 0 and 160° using a step interval of 0.05° and a step monitoring count of 95000 n using a He-3 proportional counter (32 multi-channel detector). The neutron data were collected at *in situ* temperatures of 20, 300, 450, 600 and 900ºC under vacuum. In addition, room-temperature neutron data were obtained on samples heated in an electric furnace (in air) at 400, 500, 700, 800 and 900ºC for 12 h.

Crystal structures were refined from the neutron data using the Rietveld method (Rietveld, 1969). The crystal structure data were refined using the FullProf program

(Rodriguez-Carvajal, 1998) based on the DBWS program (Wiles and Young, 1981). All refinements were performed in the $C2/m$ space group ($1M$ polytype) using the coordinate set reported by Russell and Guggenheim (1999). The atomic occupancy was initially set up according to our chemical analyses. A pseudo-Voigt function simulated the peak shape, and the FWHM (full with at half maximum) was refined with three free parameters u, v and w, depending on 2θ (Cagliotti *et al.*, 1958). The refinements included, in order, the scale factor, zero, six background, unit-cell parameters,
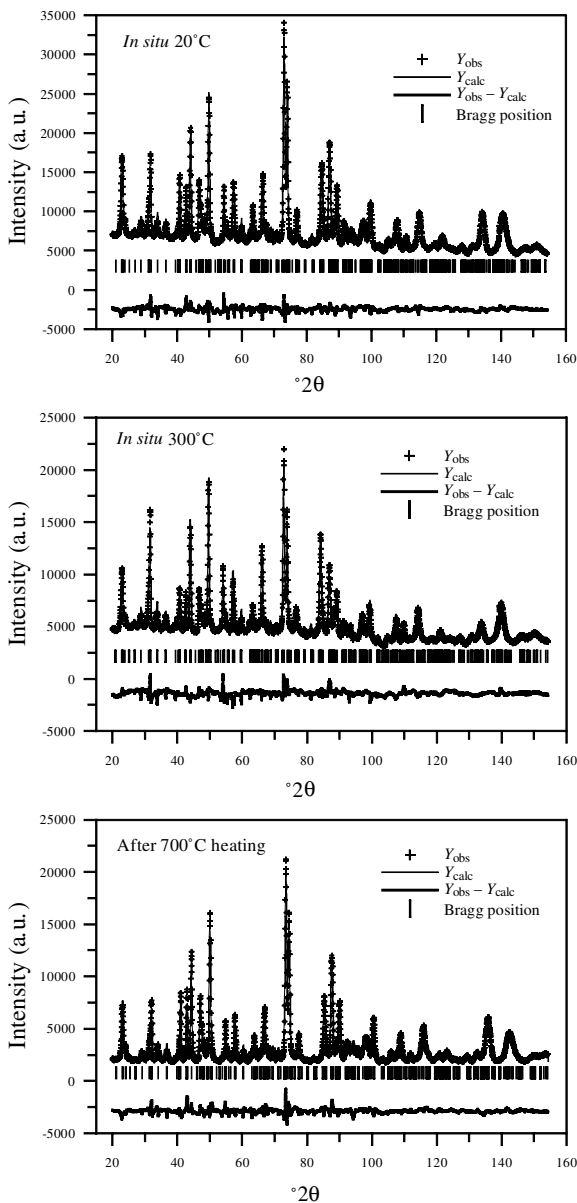

Figure 1. Observed and calculated neutron powder diffraction patterns and residuals for biotite as determined from Rietveld refinement for some experimental conditions.
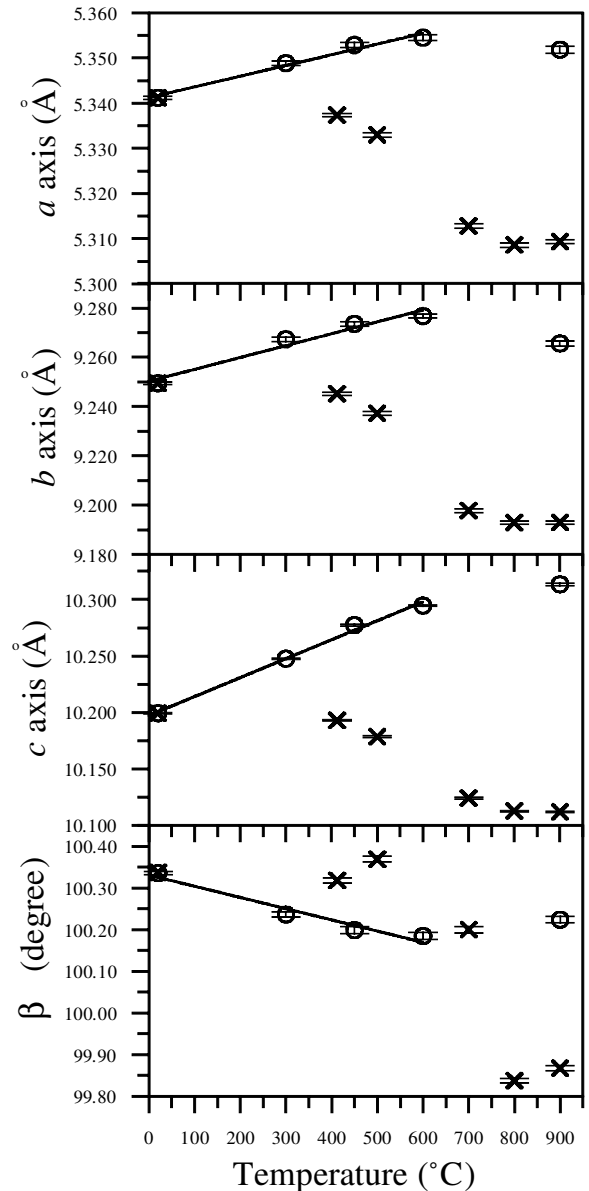

Figure 2. Plots of *a*, *b* and *c* cell parameters *vs.* temperature for samples heated in vacuum and analyzed *in situ* (circles), and for samples heated to a maximum temperature in air and analyzed at room temperature (crosses).

preferred orientation, peak shape function, and atomic coordinates. The March preferred orientation correction (Dollase, 1986) using the special direction [001] was applied to the refinement. All data below 20°2θ were excluded from profiles due to the large degree of peak asymmetry. Finally, individual thermal parameters for all atoms were considered as isotropic and refined. Cation ordering was constrained to the room temperature value since no significant change could be obtained and no regular pattern was observed among the Mg and Fe occupancies across the octahedral sites. Attempts to refine the occupancies of the (OH, F) sites were unstable, *i.e.* the values were unreasonable or diverged, except for the data from the heated samples. The refinement of the occupancies was, therefore, constrained according to the chemical analyses, but the H occupancies of the heated samples were unconstrained. The coordinates of all atoms were refined unconstrained, except for H atom positions constrained by the position at room temperature for the *in situ* high-temperature datasets.

RESULTS AND DISCUSSION

Rietveld structure refinements

The structural formula of the biotite-1M from Bancroft, Ontario, is $(K_{1.96}Na_{0.13}Ca_{0.01})(Mg_{3.15}Fe^{2+}_{2.59} Ti_{0.17}Mn_{0.09})(Si_{5.98}Al_{1.92}Ti_{0.10})O_{20}[(OH)_{1.47}F_{1.98}]$, based on the XRF and TG/DTA analyses. The experimental details and final parameters of the Rietveld structure refinements are shown in Table 1 and some graphical results of the refinements are shown in Figure 1. The 345–354 unique reflections were separated in the 20–155°2θ range at the final refinements. The reliability indexes are expressed as the various agreement factors, *e.g.* the Bragg reliability factor R_B. The crystal structure was refined to an R_P of 2.98–5.06% and R_{wp} of 3.84–6.77%. The indexes are

higher than the commonly expected values, especially with the *in situ* high-temperature data. However, it is sufficient to allow a comparison of the refinement results with each other. The final unit-cell dimensions, and atomic coordinates for all the experimental sets are shown in Tables 2 and 3, respectively. Table 4 shows the interatomic distances and some of the structure parameters as determined from a Rietveld refinement of the neutron data.

Cystal structures of biotite at high temperatures

Upon heating, the expansion of the a, b and c unit-cell dimensions occurred linearly up to 600°C. The thermal expansion in the c dimension was 1.65×10^{-5}°C^{-1}, while those along the a and b dimensions were only 4.44×10^{-6}°C^{-1} and 5.21×10^{-6}°C^{-1}, respectively (Figure 2). Therefore, the increase in the unit-cell volume was mainly due to the c axis increase up to 600°C. These changes are similar to those found by others working on neutron diffraction of micas at high temperature (Pavese *et al.*, 1997; Mookerjee *et al.*, 2001). These trends were also similar to previous high-temperature structural studies for fluorophlogopite and phlogopite using XRD (Takeda and Morosin, 1975; Russell and Guggenheim, 1999). However, the tetrahedral rotation angle, α, of biotite was smaller at all temperatures than those for fluorophlogopite (from 6.4° at 24°C to 2.7° at 700°C, Takeda and Morosin, 1975) and phlogopite (from 11.3° at 20°C to 6.7° at 600°C: Russell and Guggenheim, 1999). The lateral expansion of the octahedral sheet results in a change in the tetrahedral rotation angle, α, to accommodate the linkage between the octahedral and tetrahedral sheets. The angle decreased with increasing temperature from 3.76° at 20°C to 1.95° at 600°C, distorting the silicate ring (Figure 3a). For the phlogopites from the previous study, the octahedral thickness increased with increasing temperature, though no correlation between the octahe-

Table 2. Unit-cell dimensions of biotite after final refinement.

	In situ experiments				
T(°C)	20	300	450	600	900
a (Å)	5.3412(4)	5.3489(5)	5.3529(6)	5.3545(6)	5.3518(8)
b (Å)	9.2495(6)	9.2674(9)	9.2736(9)	9.277(1)	9.266(1)
c (Å)	10.1994(6)	10.2476(7)	10.2774(9)	10.2946(8)	10.313(1)
β (Å)	100.337(4)	100.236(6)	100.199(9)	100.184(7)	100.224(8)
V (Å^3)	495.70(6)	499.89(8)	502.11(9)	503.30(9)	503.3(1)

	Ex situ experiments				
T(°C)	400	500	700	800	900
a (Å)	5.3374(4)	5.3330(5)	5.3128(5)	5.3086(4)	5.3093(4)
b (Å)	9.2452(7)	9.2373(8)	9.1977(8)	9.1929(6)	9.1929(7)
c (Å)	10.1930(7)	10.1785(8)	10.1241(7)	10.1127(6)	10.1118(6)
β (Å)	100.318(6)	100.368(7)	100.200(8)	99.837(5)	99.867(6)
V (Å^3)	494.84(7)	493.23(8)	486.90(7)	486.26(6)	486.24(6)

Note: Esds on the last significant digit are in parentheses

Table 3. Positional coordinates and isotropic atomic displacement parameters for biotite after Rietveld refinement.

Temperature (°C)		In situ experiments					Ex situ experiments				
		20	300	450	600	900	400	500	700	800	900
T	x	0.071(1)	0.069 (2)	0.064(2)	0.068(2)	0.071(2)	0.070(2)	0.072(2)	0.071(2)	0.070(1)	0.064(2)
	y	0.1670(8)	0.164(1)	0.166(1)	0.165(1)	0.168(1)	0.1679(8)	0.1686(9)	0.1649(8)	0.1656(7)	0.1654(8)
	z	0.2240(4)	0.2227(4)	0.2218(5)	0.2234(4)	0.2273(5)	0.2238(4)	0.2243(4)	0.2239(4)	0.2233(4)	0.2233(4)
	B_{iso}	0.84(6)	1.32(8)	1.20(9)	1.29(8)	1.6(1)	1.12(6)	0.85(7)	0.68(6)	0.59(6)	0.66(7)
M1	x	0.00000	0.00000	0.00000	0.00000	0.00000	0.00000	0.00000	0.00000	0.00000	0.00000
	y	0.00000	0.00000	0.00000	0.00000	0.00000	0.00000	0.00000	0.00000	0.00000	0.00000
	z	0.50000	0.50000	0.50000	0.50000	0.50000	0.50000	0.50000	0.50000	0.50000	0.50000
	B_{iso}	0.4(1)	1.2(2)	0.1(2)	1.1(2)	2.0(2)	0.6(1)	0.6(1)	1.4(1)	1.6(1)	1.7(2)
M2	x	0.00000	0.00000	0.00000	0.00000	0.00000	0.00000	0.00000	0.00000	0.00000	0.00000
	y	0.3305(5)	0.3321(8)	0.3338(8)	0.3342(8)	0.3399(9)	0.3310(5)	0.3324(5)	0.3382(5)	0.3379(5)	0.3384(5)
	z	0.50000	0.50000	0.50000	0.50000	0.50000	0.50000	0.50000	0.50000	0.50000	0.50000
	B_{iso}	1.39(9)	1.5(1)	2.1(1)	2.1(1)	2.9(1)	1.59(9)	1.6(1)	1.57(9)	1.53(9)	1.36(9)
K	x	0.00000	0.00000	0.00000	0.00000	0.00000	0.00000	0.00000	0.00000	0.00000	0.00000
	y	0.50000	0.50000	0.50000	0.50000	0.50000	0.50000	0.50000	0.50000	0.50000	0.50000
	z	0.00000	0.00000	0.00000	0.00000	0.00000	0.00000	0.00000	0.00000	0.00000	0.00000
	B_{iso}	3.4(2)	5.2(3)	6.1(4)	6.0(4)	6.1(5)	3.8(2)	3.4(2)	2.9(2)	2.5(2)	2.5(2)
O1	x	0.041(1)	0.044(2)	0.056(2)	0.050(2)	0.038(2)	0.030(1)	0.030(1)	0.025(1)	0.028(1)	0.029(1)
	y	0.00000	0.00000	0.00000	0.00000	0.00000	0.00000	0.00000	0.00000	0.00000	0.00000
	z	0.1717(8)	0.171(1)	0.173(1)	0.173(1)	0.168(1)	0.1743(9)	0.1741(9)	0.1678(9)	0.1660(9)	0.1642(9)
	B_{iso}	1.4(2)	2.9(3)	2.5(3)	3.7(3)	4.4(4)	1.7(2)	1.3(2)	1.4(2)	1.7(2)	1.9(2)
O2	x	0.3143(9)	0.306(1)	0.304(1)	0.306(1)	0.306(2)	0.3112(9)	0.3127(9)	0.3172(9)	0.3175(9)	0.318(1)
	y	0.2405(4)	0.2424(6)	0.2438(6)	0.2437(6)	0.2444(8)	0.2410(5)	0.2409(5)	0.2372(5)	0.2349(4)	0.2344(5)
	z	0.1625(5)	0.1680(5)	0.1680(7)	0.1694(5)	0.1725(7)	0.1630(5)	0.1628(5)	0.1636(5)	0.1631(5)	0.1625(5)
	B_{iso}	2.2(1)	2.3(1)	2.1(2)	2.5(1)	3.1(2)	1.9(1)	1.9(1)	1.8(1)	1.7(1)	1.5(1)
O3	x	0.1273(9)	0.124(2)	0.121(2)	0.122(2)	0.121(2)	0.125(1)	0.126(1)	0.126(1)	0.124(1)	0.126(1)
	y	0.1665(5)	0.1665(7)	0.1663(8)	0.1665(7)	0.1698(9)	0.1676(5)	0.1686(5)	0.1686(5)	0.1670(4)	0.1673(5)
	z	0.3895(3)	0.3888(4)	0.3879(4)	0.3892(4)	0.3909(5)	0.3885(3)	0.3882(3)	0.3894(3)	0.3895(3)	0.3914(3)
	B_{iso}	0.83(6)	1.25(9)	1.02(8)	1.75(9)	2.6(1)	0.73(6)	0.74(6)	0.88(6)	0.75(6)	0.63(7)
O4	x	0.131(1)	0.128(2)	0.140(2)	0.130(2)	0.141(3)	0.134(2)	0.134(2)	0.139(2)	0.141(1)	0.142(2)
	y	0.50000	0.50000	0.50000	0.50000	0.50000	0.50000	0.50000	0.50000	0.50000	0.50000
	z	0.3959(7)	0.3954(8)	0.4025(9)	0.3971(7)	0.3984(9)	0.4042(6)	0.4049(6)	0.4010(6)	0.4005(6)	0.3986(6)
	B_{iso}	0.7(1)	0.9(1)	1.4(2)	1.2(1)	1.6(2)	0.9(1)	0.6(1)	0.18(9)	0.06(9)	0.1(1)
H	x	0.130(7)	0.130	0.130	0.130	0.130	0.49(2)	0.50(2)	0.51(2)	0.49(2)	0.46(2)
	y	0.50000	0.50000	0.50000	0.50000	0.50000	0.50000	0.50000	0.50000	0.50000	0.50000
	z	0.305(4)	0.305	0.305	0.305	0.305	0.31(1)	0.31(1)	0.31(1)	0.331(9)	0.337(8)
	B_{iso}	4.3(7)	20.1(9)	50.2(9)	31.0(9)	114(9)	23.2(9)	23.6(9)	20.1(9)	22.0(9)	17.1(9)

B_{iso}: isotropic thermal parameter
B_{ov}: overall thermal parameter
Esds on the last significant digit are in parentheses

dral thickness and increasing temperature was found in the current study (Figure 4a). The octahedral expansion of biotite at high temperatures has, therefore, only a slight effect on the c axis dominant expansion when compared to fluorophlogopite and phlogopite (Takeda and Morosin, 1975; Russell and Guggenheim, 1999). This is because the M site octahedron of biotite already becomes larger than in phlogopite as a result of Fe substitution.

For the K coordination sphere, the six inner (shortest) bonds lengthen greatly with temperature, while the other six bonds contract or do not change substantially (except at 900°C; Table 5). These findings confirm previous observations in fluorphlogopite (Takeda and Morosin,

1975), muscovite (Guggenheim et al., 1987; Catti et al., 1989), and phengite (Mookerjee and Redfern, 2002). The average coefficient of thermal expansion over all K−O bonds compares favorably with that along the c axis, so that the K plane contributes mainly to dilation along that direction.

The crystal structure deformation caused by a thermal effect can be analyzed in a similar fashion to that produced by mechanical stress (Catti, 1989). Mookerjee and Redfern (2002) developed and elucidated the formalism originally introduced by Catti (1989) to understand the strain within a crystal structure. The formalism is that the square of the distance between two atoms can be expressed in terms of $X^T G X$ where G is the

Table 4. Selected data from interatomic distances and some structure parameters (Å) for biotite as determined from Rietveld refinement of neutron powder diffraction data.

Temperature (ºC)	*In situ* experiments					*Ex situ* experiments				
	20	300	450	600	900	400	500	700	800	900
$T-O1$	1.633(8)	1.60(1)	1.61(1)	1.61(1)	1.67(1)	1.634(8)	1.642(8)	1.623(8)	1.630(7)	1.633(8)
$T-O2$	1.684(9)	1.64(1)	1.66(1)	1.65(1)	1.63(2)	1.670(9)	1.668(9)	1.675(9)	1.668(8)	1.697(9)
$T-O2'$	1.643(9)	1.67(1)	1.63(1)	1.65(1)	1.65(2)	1.640(9)	1.638(9)	1.648(9)	1.649(8)	1.631(9)
$T-O3$	1.660(5)	1.675(6)	1.680(7)	1.680(5)	1.661(7)	1.652(5)	1.642(6)	1.649(5)	1.657(5)	1.675(6)
$<T-O>$	1.655	1.65	1.65	1.65	1.65	1.649	1.647	1.649	1.651	1.659
$\alpha*$	3.757	2.940	2.777	1.949	0.936	3.568	3.604	5.085	5.959	6.151
$M1-O3[\times 4]$	2.093(5)	2.096(6)	2.095(7)	2.091(7)	2.102(8)	2.100(5)	2.107(5)	2.091(5)	2.071(4)	2.066(5)
$M1-O4[\times 2]$	2.064(8)	2.08(1)	2.01(1)	2.08(1)	2.02(1)	2.024(8)	2.018(8)	2.00(1)	1.997(7)	1.999(8)
$<M1-O>$	2.083	2.092	2.066	2.087	2.070	2.075	2.078	2.061	2.046	2.044
$M2-O3[\times 2]$	2.076(6)	2.090(8)	2.103(9)	2.103(9)	2.11(1)	2.072(6)	2.075(6)	2.097(6)	2.097(5)	2.093(6)
$M2-O3'[\times 2]$	2.105(5)	2.126(7)	2.149(8)	2.142(9)	2.14(1)	2.116(5)	2.113(5)	2.103(8)	2.116(5)	2.098(6)
$M2-O4[\times 2]$	2.084(6)	2.075(8)	2.051(9)	2.053(9)	2.04(1)	2.038(6)	2.022(6)	2.007(7)	2.013(5)	2.023(6)
$<M2-O>$	2.088	2.097	2.101	2.099	2.09	2.075	2.070	2.069	2.075	2.071
$t_{oct}**$	2.175	2.224	2.181	2.213	2.184	2.131	2.127	2.128	2.128	2.115
$\Psi_{M1}^{\dagger}$	58.53	57.89	58.13	57.97	58.25	59.10	59.21	58.92	58.66	58.84
Ψ_{M2}	58.61	57.98	58.73	58.19	58.56	59.11	59.09	59.05	59.15	59.29
$K-O1[\times 2]$	3.097(6)	3.122(9)	3.19(1)	3.16(1)	3.08(1)	3.059(7)	3.054(7)	2.996(7)	3.009(7)	3.007(8)
$K-O2[\times 4]$	3.044(5)	3.118(6)	3.136(7)	3.143(6)	3.166(7)	3.056(5)	3.048(5)	3.002(5)	2.978(5)	2.971(5)
$<K-O>_{inner}$	3.062	3.120	3.153	3.150	3.138	3.057	3.050	3.000	2.989	2.983
$K-O1[\times 2]$	3.260(6)	3.247(9)	3.21(1)	3.24(1)	3.26(1)	3.323(7)	3.319(7)	3.284(7)	3.248(7)	3.231(8)
$K-O2[\times 4]$	3.214(5)	3.216(6)	3.206(6)	3.219(6)	3.229(7)	3.204(5)	3.203(5)	3.231(5)	3.248(5)	3.249(5)
$<K-O>_{outer}$	3.229	3.226	3.208	3.227	3.240	3.244	3.242	3.249	3.248	3.243
$\Delta(K-O)$	0.167	0.107	0.055	0.079	0.102	0.186	0.192	0.249	0.259	0.260
$H-O4$	0.93(4)	0.93(9)	0.9 (2)	0.9(1)	0.9(9)	2.3(1)	2.3(9)	2.29(8)	2.07(9)	1.90(8)
Interlayer Separation	3.323	3.407	3.439	3.457	3.477	3.345	3.335	3.288	3.270	3.249
$\Psi_{Interlayer}^{\ddagger}$	57.15	56.91	56.95	56.71	56.36	56.84	56.86	56.77	56.84	57.00

* α = tetrahedral rotation angle: $\tan\alpha = \dfrac{2b(0.25 - y_{O2})}{0.5a}$

** t_{oct} = octahedral sheet thickness: $t_{oct} = 2\left(0.5 - \dfrac{2(Z_{O3}) + Z_{OH}}{3}\right)c_0\sin\beta$

$^{\dagger}\Psi_M$ = octahedral flattening angle: $\cos\Psi = \dfrac{t_{oct}}{2d_0}$

d_0 = mean $<M-O>$ distance (according to Hazen and Burnham, 1973)

$^{\ddagger}\Psi_{Interlayer}$ = K-octahedral flattening angle: $\cos\Psi = \dfrac{(K-octahedral\ thickness)}{2(mean\ <K-O>_{inner}\ distance)}$ (according to Takeda and Donnay, 1966)

Esds on the last significant digit are in parentheses. Bond multiplicities are given in brackets.

metric matrix (the determinant of which gives the square of the unit-cell volume) and X represents the fractional coordinates of the atom under consideration. The differences in the square of the distance can, therefore, be expressed in the terms separated into inner strain and external (lattice) strain components (Mookerjee and Redfern, 2002). It is well known that when an homogeneous elastic stress induces the deformation of a crystal structure, the structure preserves translational symmetry and can be considered as the superposition of an external (lattice) strain and internal strain (Born and Huang, 1954). The external strain describes the change in the lattice parameters. The internal strain describes the change in the fractional coordinates of atoms. Applying the above to the K–O bonds in our results, except for 900ºC (Table 5), which shows anisotropy in

the interlayer region, we find that the six long bonds have a negative inner strain component and the six short bonds have a positive strain component. A positive inner strain contribution indicates that the bond expands by more than expected from unit-cell dilation alone, whereas the opposite is implied by a negative value. Thus, in the interlayer region (K coordination sphere), a large effect due to inner thermal strain is observed, indicating the dominance of the inner deformation over the external deformation. In contrast, for the long K–O2 bonds, lattice deformation seems to dominate the inner deformation, maintaining the trend of the other short bonds.

An ideal octahedron has an angle, Ψ, of 54.73º and this angle is measured between the body diagonal and the normal to the top plane. If the angle is greater than
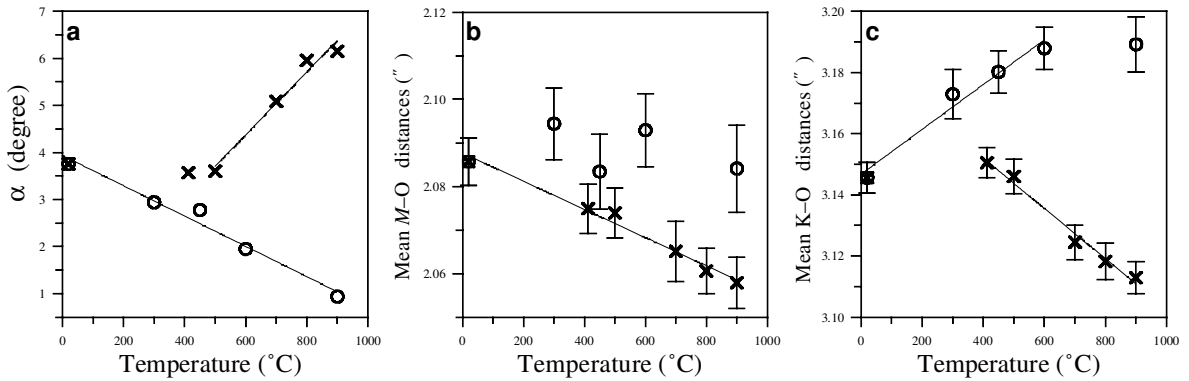
Figure 3. Plots of (a) α (tetrahedron rotation angle), (b) mean $<M-O>$ and (c) mean $<K-O>$ distance *vs*. temperature for samples heated in vacuum and analyzed *in situ* (circles), and for samples heated to a maximum temperature in air and analyzed at room temperature (crosses).

the ideal value, the octahedron is flattened, and octahedral thickness is then reduced (Hazen and Burnham, 1973). The interlayer-K octahedron in biotite, using nearest-neighbor anions, had a flatter shape (20°C: 57.15°; 900°C: 56.61°) than an ideal octahedron because of the attractive forces between K^+ and F^-. The interlayer octahedral flattening angle, $\Psi_{interlayer}$, decreased with increasing temperature, with an accompanying elongation of the K site and an increase in the interlayer separation (thickness) (Figure 4c). This decrease in $\Psi_{interlayer}$ also indicates that the *c*-axis dominant expansion of biotite at high temperatures does not derive from octahedral expansion but from interlayer expansion and elongation along the *c* axis.

The expansion of unit-cell dimensions at 900°C showed a different trend from that at lower temperatures. The *a* and *b* dimensions decreased slightly at higher temperatures rather than increased as observed at lower temperatures. This may be attributed to a change in the octahedral dimension caused by a dehydroxylation-oxidation reaction of Fe^{2+} to Fe^{3+} in vacuum conditions at the higher temperatures (Tripathi *et al.*, 1978). Mookerjee *et al.* (2001) suggested, however, that the

reduction of the cell dimensions at the highest temperatures might not be caused by oxidation on heating. They also found an apparent decrease at 700°C, the highest temperature of their experiment. Their sample was heated in a vanadium vessel. Since vanadium acts as a highly efficient 'oxygen-getter', it is extremely unlikely that the sample was oxidized at all on heating. We also used a vanadium vessel, which could have prevented biotite oxidation at the highest temperature, and therefore it might give rise to the apparent reduction in the cell dimensions.

Crystal structures of heat-treated biotite

In contrast to the results of *in situ* heating experiments, the unit-cell lengths of the heat-treated samples in air decreased up to 800°C, when compared with those of the untreated sample (Figure 2). The trends observed in this study confirm the trends reported in previous studies on mica, although the magnitudes differed according to the Fe concentration (Takeda and Ross, 1975; Ohta *et al.*, 1982; Russell and Guggenheim, 1999). A decrease in the mean $<M-O>$ distance and the octahedral sheet thickness, t_{oct}, from the untreated
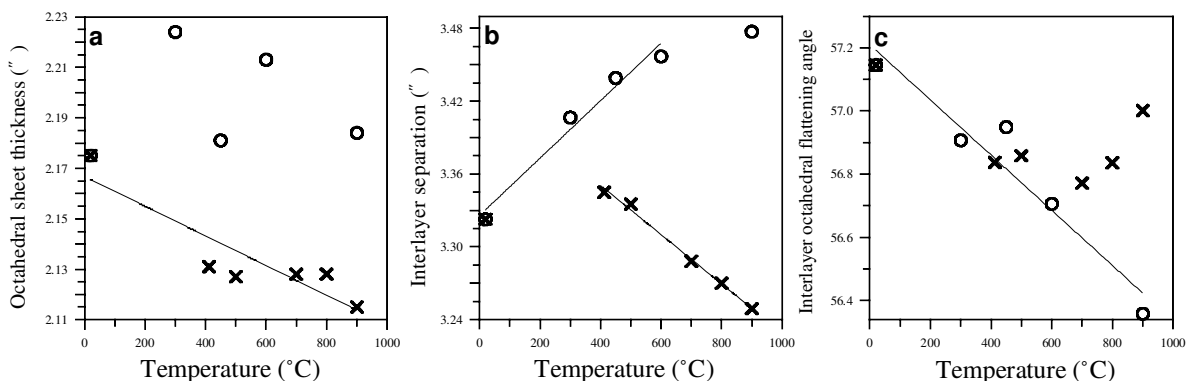

Figure 4. Plots of (a) octahedral sheet thickness, (b) interlayer separation, and (c) interlayer octahedral flattening angle *vs*. temperature for samples heated in vacuum and analyzed *in situ* (circles), and for samples heated to a maximum temperature in air and analyzed at room temperature (crosses).

Table 5. Bond lengths, changes of squared bond lengths Δ, (I) their lattice components and (II) the component of inner deformation are reported for K–O bonds.

In situ	Bond length (Å) at 20°C	Bond length (Å) at 600°C	Δ (Å^2)	I	II	ε ($10^{-5°}$C^{-1})
$(K-O1)_{inner}$ [× 2]	3.097(6)	3.16(1)	0.41	0.11	0.30	11.2
$(K-O2)_{inner}$ [× 4]	3.044(5)	3.143(6)	0.63	0.08	0.55	17.5
$(K-O1)_{outer}$ [× 2]	3.260(6)	3.24(1)	−0.12	0.08	−0.20	−3.09
$(K-O2)_{outer}$ [× 4]	3.214(5)	3.219(6)	0.01	0.10	−0.09	0.29
$<K-O>_{mean}$	3.145(6)	3.188(4)				2.33

Ex situ	at 400°C	at 900°C	Δ (Å^2)	I	II	ε ($10^{-5°}$C^{-1})
$(K-O1)_{inner}$ [× 2]	3.059(7)	3.007(8)	−0.32	−0.03	−0.29	−10.5
$(K-O2)_{inner}$ [× 4]	3.056(5)	2.971(5)	−0.52	−0.14	−0.38	−14.5
$(K-O1)_{outer}$ [× 2]	3.323(7)	3.231(8)	−0.61	−0.21	−0.40	−16.0
$(K-O2)_{outer}$ [× 4]	3.204(5)	3.249(5)	0.29	−0.08	0.37	7.83
$<K-O>_{mean}$	3.151(6)	3.113(7)				−2.38

ε is the linear thermal expansion of each band
Δ ($d'_{KO}{}^2 - d_{KO}{}^2 = I + II$) is the difference in the K–O bond length
$I = (x_K - x_O)^T \Delta G (x_K - x_O)$ is the contribution of pure lattice deformation
$II = [(x_K - x_O)^T G'(\Delta x_K - \Delta x_O) + (\Delta x_K - \Delta x_O)^T G'(x_K - x_O) + (\Delta x_K - \Delta x_O)^T G'(\Delta x_K - \Delta x_O)]$ is the strain entirely related to inner deformation (according to Catti *et al.*, 1989; Mookherjee and Redfern, 2002).
The x_K and x_O are the sectors of the fractional coordinates of the atom, respectively, with respect to a common origin and G is the metric matrix (the determinant of which gives the square of the unit-cell volume).
Esds on the last significant digit are in parentheses. Bond multiplicities are given in brackets.

sample was observed (Figures 3b, 4a). This structural contraction of the heat-treated biotite is attributed to oxidation and dehydroxylation. With increasing temperature, dehydroxylation continues alongside oxidation, beginning at below 400°C in an oxidizing environment and above 800°C in an oxygen-poor environment (Hogg and Meads, 1975). Reductions in the mean $<M-O>$ distance and t_{oct} appear to be caused by a change in the cation size from Fe^{2+} to Fe^{3+} due to octahedral Fe oxidation. This contraction in the octahedral sheet thickness results in an increase in the tetrahedral rotation angle, α, to accommodate the lateral misfit between the octahedral and tetrahedral sheets (Figure 3a). However, in the 400°C treated sample, the mean $<K-O>$ distance and the interlayer separation in relation to interlayer dimensions decreased linearly (Figures 3c, 4b). This trend may be due to the dehydroxylation that began at ~400°C. The overall cell dimensions also decreased rapidly as the temperature increased from 400 to 700°C. This suggests that the reduction in the cell dimensions at temperatures from ~400°C is mainly due to the effect of dehydroxylation in the crystal structure as a result of heating in air. Confirmation of this suggestion was attempted by using the refined occupancy of the H site, but no significant change could be obtained among the occupancies, except a small reduction at 900°C. Reduction in the unit-cell parameter was insignificant at 800 and 900°C, while the mean $<K-O>$ distance and the interlayer separation decreased linearly up to 900°C; therefore, the β angles had significantly low values at 800 and 900°C (Figure 2).

The reduction in the interlayer dimensions occurs because of a weakening interaction of the repulsive forces between the interlayer K^+ and the H^+, which resulted from dehydroxylation (Ohta *et al.*, 1982). In addition, owing to the attractive forces between K^+ and F^-, the interlayer coordination sphere was compressed along the c axis (Russell and Guggenheim, 1999). The deformation of the K–O bonds in the interlayer region can be separated into a lattice strain and an inner strain contribution (Table 5). A negative inner strain component indicates that the bond contracts more than expected from unit-cell reduction alone, whereas the opposite is implied by a positive value. The large inner strains observed upon the contraction of K–O bonds in the heated biotite considerably increased ditrigonal distortion (3.57° at 400°C to 6.15° at 900°C) and confirmed the previous findings of Ohta *et al.* (1982) and Russell and Guggenheim (1999). The average coefficient of the contraction over all K–O bonds compares favorably with that along the c axis ($-1.81 \times 10^{-5°}$C^{-1}), so the K plane contraction evidently controls the reduction along that direction (Table 5).

CONCLUSIONS

In this study, an attempt was made to determine the significance of the variations in the structural parameters as a result of the high-temperature experiments using neutron powder diffraction. The changes in crystal structure parameters as the experimental conditions were varied were related to mechanisms of Fe oxidation

and dehydroxylation. The increase in the unit-cell volume with *in situ* heating in vacuum at temperatures up to 600°C occurred mainly along the *c* axis, as a result of expansion in the K coordination sphere along that direction. The ditrigonal distortion decreased (3.76° at 20°C to 1.95° at 600°C) with temperature, because the shorter bonds expanded and the longer contacts contracted. The increase in the interlayer separation and the decrease in the flattening angle of the interlayer octahedron confirmed that the *c* axis-dominated expansion derived mainly from the interlayer region.

In the case of heat-treated biotite in an oxidizing environment, the cell dimensions decreased up to 700°C. This decrease in the dimension was attributed to the mixed effect of octahedral Fe oxidation and dehydroxylation. This study did not determine how the octahedral Fe was oxidized directly. However, the linear reduction in the octahedral dimension suggests indirectly that octahedral Fe oxidation continues with increasing temperatures in all heat-treated samples. The average coefficient of the contraction over all K–O bonds compares favorably with that along the *c* axis at temperatures above 400°C. This suggests that the reduction in the interlayer region by dehydroxylation controls the variation in the overall cell parameters with temperature. The large inner strain components in the K–O bonds also increased the ditrigonal distortion (3.57° at 400°C to 6.15° at 900°C).

ACKNOWLEDGMENTS

REFERENCES

Akiba, E., Hayakawa, H., Hayashi, S., Miyawaki, R. and Tomura, S. (1997) Structure refinement of synthetic deuterated kaolinite by Rietveld analysis using time-of-flight neutron powder diffraction data. *Clays and Clay Minerals*, **45**, 781–788.

Bigi, S. and Brigatti, M.F. (1994) Crystal chemistry and microstructures of plutonic biotite. *American Mineralogist*, **79**, 63–72.

Bish, D.L. (1993) Rietveld refinement of the kaolinite structure at 1.5 K. *Clays and Clay Minerals*, **41**, 738–744.

Bohlen, S.R., Peacor, D.R. and Essene, E.J. (1980) Crystal chemistry of a metamorphic biotite and its significance in water barometry. *American Mineralogist*, **65**, 55–62.

Born, M. and Huang, K. (1954) *Dynamical Theory of Crystal Lattices*. Clarendon Press, Oxford, UK.

Brigatti, M.F. and Davoli, P. (1990) Crystal-structure refinements of 1M plutonic biotites. *American Mineralogist*, **75**, 305–313.

Cagliotti, G., Paoletti, A. and Ricci, F. (1958) Choice of collimators for a crystal spectrometer for neutron diffraction. *Nuclear Instruments*, **3**, 223–228.

Catti, M. (1989) Calculation of elasticity and inner strain: a computational model. *Acta Crystallographica*, **A45**, 494–500.

Catti, M., Ferraris, G. and Ivaldi, G. (1989) Thermal strain analysis in the crystal structure of muscovite at 700°C. *European Journal of Mineralogy*, **1**, 625–632.

Catti, M., Ferraris, G., Hull, S. and Pavese, A. (1994) Powder neutron diffraction study of 2M₁ muscovite at room pressure and at 2 GPa. *European Journal of Mineralogy*, **6**, 171–178.

Dollase, W.A. (1986) Correction of intensities for preferred orientation in powder diffractometry: Application of the march model. *Journal of Applied Crystallography*, **19**, 267–272.

Guggenheim, S., Chang, Y.-H. and Koster Van Groos, A.F. (1987) Muscovite dehydroxylation: High-temperature studies. *American Mineralogist*, **72**, 537–550.

Hazen, R.M. and Burnham, C.W. (1973) The crystal structure of one-layer phlogopite and annite. *American Mineralogist*, **58**, 889–900.

Hogg, C.S. and Meads, R.E. (1975) A Mössbauer study of thermal decomposition of biotites. *Mineralogical Magazine*, **40**, 79–88.

Joswig, W. (1972) Neutronenbeugungsmessungen an einem 1*M*-Phlogopit. *Neues Jahrbuch fur Mineralogie Monatshefte, Niemcy*, 1–11.

Joswig, W., Fuess, H. and Rothbauer, R. (1980) A neutron diffraction study of a one-layer triclinic chlorite (penninite). *American Mineralogist*, **65**, 349–352.

Liang, J.J. and Hawthorne, F.C. (1998) Triclinic muscovite: X-ray diffraction, neutron diffraction and photo-acoustic FTIR spectroscopy. *The Canadian Mineralogist*, **37**, 1017–1027.

Mookerjee, M. and Redfern, S.A.T. (2002) A high-temperature Fourier transform infrared study of the interlayer and Si–O-stretching region in phengite-2M₁. *Clay Minerals*, **37**, 323–336.

Mookerjee, M., Redfern, S.A.T. and Zhang, M. (2001) Thermal response of structure and hydroxyl ion of phengite-2M₁: an *in situ* neutron diffraction and FTIR study. *European Journal of Mineralogy*, **13**, 545–555.

Ohta, T., Takeda, H. and Takéuchi, Y. (1982) Mica polytypism: similarities in the crystal structures of 1M and 2M1 oxybiotite. *American Mineralogist*, **67**, 298–310.

Pavese, A., Ferraris, G., Prencipe, M. and Ibberson, R. (1997) Cation site ordering in phengite 3T from the Dora-maira massif (Western Alps): A variable-temperature neutron powder diffraction study. *European Journal of Mineralogy*, **9**, 1183–1190.

Pavese, A., Ferraris, G., Pischedda, V. and Ibberson, R. (1999) Tetrahedral order in thermodynamic consequences. *European Journal of Mineralogy*, **11**, 309–320.

Pavese, A., Ferraris, G., Pischedda, V. and Radaelli, P. (2000) Further study of the cation ordering in phengite 3T by neutron powder diffraction. *Mineralogical Magazine*, **64**, 11–18.

Pavese, A., Ferraris, G., Pischedda, V. and Fauth, F. (2001) M1-site occupancy in 3T and 2M(1) phengites by low temperature neutron powder diffraction: Reality or artifact? *European Journal of Mineralogy*, **13**, 1071–1078.

Rancourt, D.G., Christie, I.A.D., Lamarche, G., Swainson, I. and Flandrois, S. (1994) Magnetism of synthetic and natural annite mica: ground state and nature of excitations in an exchange-wise two-dimensional easy-plane ferromagnet with disorder. *Journal of Magnetism and Magnetic Materials*, **138**, 31–44.

Rancourt, D.G., Mercier, P.H.J., Cherniak, D.J., Desgreniers, S., Kodama, H. and Robert, J.-L. (2001) Mechanisms and crystal chemistry of oxidation in annite: Resolving the hydrogen-loss and vacancy reactions. *Clays and Clay Minerals*, **49**, 455–491.

Rayner, J.H. (1974) The crystal structure of phlogopite by neutron diffraction. *Mineralogical Magazine*, **39**, 850–856.

Rietveld, H.M. (1969) A profile refinement method for nuclear

and magnetic structures. *Journal of Applied Crystallography*, **2**, 65–71.

Rodriguez-Carvajal, J. (1998) *FullProf: Rietveld profile matching and integrated intensity refinement of X-ray and neutron data (PC-version).* Version 3.5d.

Russell, R.L. and Guggenheim, S. (1999) Crystal structures of near-end-member phlogopite at high temperatures and heat-treated Fe-rich phlogopite: The influence of the O, OH, F site. *The Canadian Mineralogist*, **37**, 711–729.

Takeda, H. and Donnay, J.D.H (1966) Trioctahedral one-layer micas. III. Crystal structure of a synthetic lithium fluormica. *Acta Crystallographica*, **20**, 638–646.

Takeda, H. and Morosin, B. (1975) Comparison of observed and predicted structural parameters of mica at high temperature. *Acta Crystallographica*, **B31**, 2444–2452.

Takeda, H. and Ross, M. (1975) Mica polytypism: dissimilarities in the crystal structures of coexisting 1*M* and 2*M*1

biotite. *American Mineralogist*, **60**, 1030–1040.

Tripathi, R.P., Chandra, U., Chandra, R. and Lokanathan, S. (1978) A Mössbauer study of the effect of heating biotite, phlogopite and vermiculite. *Journal of Inorganic Nuclear Chemistry*, **40**, 1293–1298.

Virgo, D. and Popp, R.K. (2000) Hydrogen deficiency in mantle-derived phlogopites. *American Mineralogist*, **85**, 753–759.

Wiles, D.B. and Young, R.A. (1981) A new computer program for Rietveld analysis of X-ray powder diffraction patterns. *Journal of Applied Crystallography*, **14**, 149–151.

Young, R.A. (1993) *The Rietveld Method.* International Union of Crystallography, Oxford University Press, Oxford, UK, 298 pp.